


Longitudinal and transverse modes of temperature-modulated inclined layer convectionJitender Singh *Department of Mathematics, Guru Nanak Dev University, Amritsar-143005, Punjab, India* (Received 13 August 2022; revised 12 January 2023; accepted 6 April 2023; published 27 April 2023)

A parametric instability of an incompressible, viscous, and Boussinesq fluid layer bounded between two parallel planes is investigated numerically. The layer is assumed to be inclined at an angle with the horizontal. The planes bounding the layer are subjected to a time-periodic heating. Above a threshold value, the temperature gradient across the layer leads to an instability of an initially quiescent state or a parallel flow, depending upon the angle of inclination. Floquet analysis of the underlying system reveals that under modulation, the instability sets in as a convective-roll pattern executing harmonic or subharmonic temporal oscillations, depending upon the modulation, the angle of inclination, and the Prandtl number of the fluid. Under modulation, the onset of the instability is in the form of one of two spatial modes: the longitudinal mode and the transverse mode. The value of the angle of inclination for the codimension-2 point is found to be a function of the amplitude and the frequency of modulation. Furthermore, the temporal response is harmonic, or subharmonic, or bicritical depending upon the modulation. The temperature modulation offers good control of time-periodic heat and mass transfer in the inclined layer convection.

DOI: [10.1103/PhysRevE.107.045104](https://doi.org/10.1103/PhysRevE.107.045104)**I. INTRODUCTION**

Inclined layer convection (ILC) is the hydrodynamic problem of instability in a differentially heated layer of a viscous, incompressible, and Newtonian fluid bounded between two parallel planes inclined at some angle with the horizontal [1–8]. The onset of ILC is generally of two types:

(i) The buoyancy-dominated instability associated with the well-studied Rayleigh-Bénard convection (RBC) in an initially quiescent horizontal fluid layer [9–12].

(ii) The dynamic shear-dominated natural convection in a vertical layer (VLC) [13–18].

As the angle of inclination of the fluid layer with the horizontal varies from zero, the mechanism of the onset of ILC is of RBC type up to an inclination of about 71° beyond which the instability mechanism is of VLC type [19].

In [3], Sparrow and Husar carried out experimental studies on ILC and found that for the considered range of inclinations, the onset of ILC in air is in the form of longitudinal rolls. Further, in another experimental work, Lloyd and Sparrow [4] determined the dependence of the Rayleigh number for the onset of ILC on the inclination of the fluid layer. It was found that for the inclination of the fluid layer with the horizontal up to 73° , the instability is characterized by longitudinal vortices, while for an inclination beyond 76° , the instability is characterized by transverse vortices, where for inclinations between 73° and 76° a transition occurs between the two modes of the instability.

These results were further confirmed by experimental and detailed theoretical work of Hart [19] on ILC with an excellent agreement between theory and experiment.

Clever and Busse [7] performed a numerical study on the stability analysis of longitudinal rolls in ILC and found a possibility of three types of transitions from the longitudinal rolls to the three-dimensional form of convection, depending upon the inclination of the fluid layer.

Hideo [8] studied experimentally the flow and heat transfer behavior of ILC in a finite box of large aspect ratio revealing a good agreement with the past theoretical studies.

Daniels *et al.* [20] performed experiments on ILC for a fluid of Prandtl number 1 and found many new interesting nonlinear chaotic states. These findings have been found to be in agreement with the recent numerical work of Subramanian *et al.* [21], Reetz and Schneider [22], Reetz *et al.* [23], and Tuckerman [24] on ILC, where a variety of spatiotemporal patterns have been found to be exhibited by ILC for fluids having Prandtl number near unity.

A rich variety of patterns exhibited by ILC as evident from the aforementioned experimental and theoretical research demonstrates the importance of ILC for further scientific investigations. Moreover, ILC has served as a model problem for practical utility from microscale to megascale in a number of heat transfer, material processing, and other industrial applications [25].

The heat and mass transfer characteristics of thermal convection in ILC can be controlled by an external time-periodic forcing of the bounding planes. The practical utility of the temperature-modulated ILC (TMILC) offers a good control of time-periodic heat and mass transfer. In fact, TMILC has a wide range of applications in the processes where rapid heat and mass transfer are required (e.g., designing heat sinks for cooling of electronic devices, heat exchangers in nuclear reactors, air conditioning, microwaves, etc.) In view of this, the parametric excitation of Faraday instability [26–29], RBC under time-periodic temperature modulation [12,30–

*<https://sites.google.com/view/sonumaths3/home>;
sonumaths@gmail.com

36] or gravity modulation [37–40], and time-periodic temperature or gravity modulation of VLC [41–43] are known to execute harmonic or subharmonic oscillations at the onset of the instability, depending upon the modulation and Prandtl number of the fluid. Rayleigh-Bénard convection is known to exhibit quasiperiodic patterns under gravity modulation [38]. The literature on these themes is vast, and the reader is referred to the excellent review in [12,44,45]. Each of these time-periodic modulation types can lead to advancement or delay of the onset of convection in different parametric ranges of the frequency and the amplitude of modulation.

Using Floquet theory, Singh and Bajaj [42] performed a linear instability analysis of VLC under time-periodic modulation of the temperatures of the vertical planes bounding the layer for fluids with Prandtl number < 12.5 . In addition to the destabilizing and stabilizing effects of modulation parameters on the onset of the instability, the onset of the instability was found to be either a harmonic or a subharmonic mode, where the mode switching always occurs through an intermediate bicritical state. For a particular combination of amplitude and frequency of forcing, the bicritical state may correspond to coexistence of a pair of either purely harmonic modes, or purely subharmonic modes, or one harmonic and one subharmonic mode. Furthermore, for fluids with Prandtl number < 12.5 , Singh *et al.* [43] have found a much wider parameter space for observing bicritical states exhibited by the temperature-modulated VLC under two-frequency forcing of the temperatures of the vertical planes bounding the layer.

Only the two particular configurations of TMILC, that is, the temperature-modulated RBC and the temperature-modulated VLC, have been investigated in detail in the recent past [42,43], which restricts its application in the case of a tilted configuration of the layer. This serves as a motivation for the present work for investigating the hydrodynamic behavior of TMILC for all possible configurations. So, in the present paper, within the framework of linear instability theory, we examine TMILC for fluids with Prandtl number < 12.5 under single-frequency time-periodic excitation of the temperatures of the two planes bounding the fluid layer. Floquet theory is utilized for this purpose.

The paper is organized as follows. The problem and the basic state are discussed in Sec. II, where a linear instability analysis of the basic state is carried out. In Sec. III, Floquet analysis of the underlying linear system is performed, and the problem is reduced to an equivalent generalized eigenvalue problem for the control parameter. Most of the numerical results are discussed in Sec. IV for the Prandtl number of air. The effect of Prandtl number on the angle of inclination corresponding to the codimension-2 point in TMILC is discussed separately in Sec. V. The conclusions are presented in Sec. VI.

II. MATHEMATICAL FORMULATION

We consider a layer of thickness $d > 0$ of a viscous, incompressible, and Newtonian fluid between two rigid parallel planes inclined at an angle β with respect to the horizontal. Aligning the coordinate system with the fluid layer as shown in Fig. 1, the planes bounding the layer are $z = -d/2$

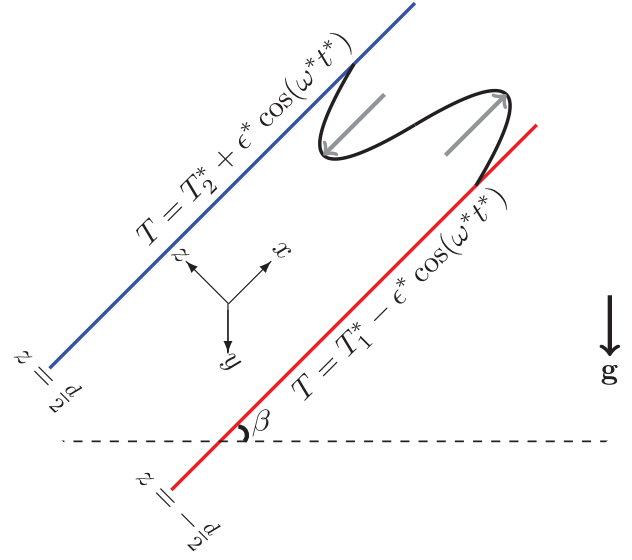


FIG. 1. Geometry of TMILC.

$d/2$, which are maintained at temperatures $T_1^* - \epsilon^* \cos(\omega^* t^*)$ and $T_2^* + \epsilon^* \cos(\omega^* t^*)$, respectively, with the base frequency $\omega^* > 0$ and amplitude of modulation $\epsilon^* \geq 0$, such that $T_1^* > T_2^* \geq 0$.

We introduce the scales to measure length, time, velocity, pressure, and temperature as d , d^2/κ , κ/d , $\rho_0 \kappa^2/d^2$, and $\Delta T^* = T_1^* - T_2^*$, respectively, where κ is the thermal diffusivity of the fluid, and ρ_0 is the density of the fluid at temperature $T_0^* = (T_1^* + T_2^*)/2$. Using these scales in the laws of conservation of mass, momentum, and energy, we obtain the Grashof number $Gr = \alpha d^3 \rho_0^2 g \Delta T^* / \eta^2$, the Prandtl number $\sigma = \eta / (\rho_0 \kappa)$, the amplitude of modulation $\epsilon = \epsilon^* / \Delta T^*$, and the basic frequency of modulation $\omega = d^2 \omega^* / \kappa$ as the four dimensionless parameters governing the flow, where g and η denote the gravitational acceleration and the dynamic viscosity of fluid, respectively. The Grashof number is related to the Rayleigh number Ra by $Ra = \sigma Gr$. In addition, $\alpha = \frac{1}{\rho_0} \frac{\partial \rho}{\partial T^*}$, where the fluid density ρ at any temperature T^* is given by the equation of state as follows:

$$\rho = \rho_0 \{1 - \alpha(T^* - T_0^*)\}. \quad (1)$$

In view of the aforementioned scaling, we further scale the temperature field within the layer so that

$$T = (T^* - T_0^*) / \Delta T^* \quad (2)$$

is the dimensionless form of the temperature. So, mathematically the working domain of the fluid layer is the set $\mathcal{D} = \mathbb{R} \times \mathbb{R} \times (-\frac{1}{2}, \frac{1}{2})$. The basic state in dimensionless form consists of the basic velocity field $(\sigma Gr V_e(z, t) \sin \beta, 0, 0)$ obeying zero net flux $\int_{-1/2}^{1/2} V_e(z, t) dz = 0$, the basic temperature field $T = T_e(z, t)$, and the basic pressure $P = P_e(x, z, t)$

associated with the fluid layer, which are given as follows:

$$V_e(z, t) = \frac{z}{6} \left(z^2 - \frac{1}{4} \right) + \epsilon \sigma \operatorname{Re} \left\{ \frac{f_1(z, \omega) - f_\sigma(z, \omega)}{(1 - \sigma)\iota\omega} e^{\iota\omega t} \right\}, \quad (3a)$$

$$T_e(z, t) = -z + \epsilon \operatorname{Re} \{ f_1(z, \omega) e^{\iota\omega t} \}, \quad (3b)$$

$$P_e(x, z, t) = P_e(-1/2) - \frac{d^3 g}{\kappa^2} (z \cos \beta + x \sin \beta) - \sigma^2 \operatorname{Gr} \cos \beta \int_{-1/2}^z T_e(s, t) ds, \quad (3c)$$

where $\operatorname{Re}[\cdot]$ denotes the real part of $[\cdot]$, and

$$f_\sigma(z, \omega) = \sinh\{\sqrt{\iota\omega/\sigma}z\}/\sinh\{(1/2)\sqrt{\iota\omega/\sigma}\}, \quad (4)$$

where we have $f_1 = f_\sigma|_{\sigma=1}$.

Considering small perturbations in (3a)–(3c) so that the perturbed velocity $(\sigma \operatorname{Gr} V_e \sin \beta, 0, 0) + (u, v, w)$, the perturbed temperature $T_e + \theta$ and the perturbed pressure $P_e + P$ satisfy the governing equations subject to the no-slip conditions at the rigid walls; the small perturbations u, v, w, θ, P after retaining linear terms and eliminating u, v , and the pressure term P from the governing equations lead to the following partial differential equations (PDEs) along with the relevant boundary conditions:

$$\frac{1}{\sigma} \frac{\partial \nabla^2 w}{\partial t} + \operatorname{Gr} \sin \beta \left(V_e \nabla^2 - \frac{\partial^2 V_e}{\partial z^2} \right) \frac{\partial w}{\partial x} = \nabla^4 w - \sigma \operatorname{Gr} \sin \beta \frac{\partial^2 \theta}{\partial x \partial z} + \sigma \operatorname{Gr} \cos \beta \left(\frac{\partial^2 \theta}{\partial x^2} + \frac{\partial^2 \theta}{\partial y^2} \right), \quad (5a)$$

$$\frac{\partial \theta}{\partial t} + w \frac{\partial T_e}{\partial z} + \sigma \operatorname{Gr} \sin \beta V_e \frac{\partial \theta}{\partial x} = \nabla^2 \theta, \quad \left(w, \frac{\partial w}{\partial z}, \theta \right) \Big|_{z=\pm \frac{1}{2}} = (0, 0, 0), \quad (5b)$$

where (5a)–(5b) depend on z and t via the boundary conditions and the basic-state velocity V_e and temperature T_e .

III. METHOD OF SOLUTION

In view of the fact that the perturbations remain bounded on \mathcal{D} and periodic in x and y , and t , we expand w and θ in the following appropriate Fourier-Floquet form [9,46]:

$$w = \sum_{\ell=-L}^L \sum_{n=1}^N \{ a_{n\ell} \Phi_n(z) + \iota b_{n\ell} \Psi_n(z) \} E_\ell(t, \mathbf{x}), \quad (6a)$$

$$\theta = \sum_{\ell=-L}^L \sum_{n=1}^N \{ \iota c_{n\ell} \mathcal{S}_n(z) + d_{n\ell} \mathcal{C}_n(z) \} E_\ell(t, \mathbf{x}), \quad (6b)$$

where

$$E_\ell(t, \mathbf{x}) = e^{\iota(s+\ell)\omega t} e^{\iota \mathbf{k} \cdot \mathbf{x}}, \quad \mathbf{x} = (x, y, 0),$$

and $\mathbf{k} = (k \cos \gamma, k \sin \gamma, 0)$ for $0^\circ \leq \gamma \leq 90^\circ$ is the wave vector of perturbations with the wave number $k > 0$, and the number of Galerkin terms N in the above expansions is chosen large enough to achieve numerical convergence within specified tolerance. Furthermore, $s = 0$ and $1/2$ correspond to the harmonic and the subharmonic responses of the perturbations,

respectively, wherein the growth rate has been set to zero in order to obtain the critical value for the control parameter for the onset of the instability. For each n , the functions $\Phi_n, \Psi_n, \mathcal{S}_n$, and \mathcal{C}_n , which are known as Chandrasekhar functions [9], obey the given Dirichlet and Newman boundary conditions imposed on w and Dirichlet boundary conditions imposed on θ , and they are defined as

$$\Phi_n(z) = \frac{\cosh \lambda_n z}{\cosh \frac{\lambda_n}{2}} - \frac{\cos \lambda_n z}{\cos \frac{\lambda_n}{2}},$$

$$\Psi_n(z) = \frac{\sinh \mu_n z}{\sinh \frac{\mu_n}{2}} - \frac{\sin \mu_n z}{\sin \frac{\mu_n}{2}},$$

$$\mathcal{S}_n(z) = \sin\{2n\pi z\}, \quad \mathcal{C}_n(z) = \cos\{(2n - 1)\pi z\},$$

where λ_n and μ_n satisfy the following:

$$\tan \frac{\lambda_n}{2} + \tanh \frac{\lambda_n}{2} = 0, \quad \cot \frac{\mu_n}{2} - \coth \frac{\mu_n}{2} = 0.$$

Substituting the truncated expansions for w and θ from (6a)–(6b) into (5a)–(5b) and performing Galerkin operations by taking unity as the weight function, we obtain the following:

$$\{ \mathbf{L}_\ell - \sigma \operatorname{Gr} (\mathbf{U}_1 \cos \beta + \mathbf{U}_2 \sin \beta \cos \gamma) \} \zeta_\ell - \epsilon (\mathbf{V} + \sigma \operatorname{Gr} \sin \beta \cos \gamma \mathbf{W}) \zeta_{\ell-1} - \epsilon (\bar{\mathbf{V}} + \sigma \operatorname{Gr} \sin \beta \cos \gamma \bar{\mathbf{W}}) \zeta_{\ell+1} = 0, \quad (7)$$

where each of $\mathbf{L}_\ell, \mathbf{U}_1, \mathbf{U}_2, \mathbf{V}$, and \mathbf{W} is a square matrix as defined in the Appendix, and $\bar{\mathbf{V}}$ (respectively $\bar{\mathbf{W}}$) is the complex conjugate of \mathbf{V} (respectively \mathbf{W}). Further, for each ℓ

$$\zeta_\ell = (a_{1\ell}, \dots, a_{N\ell}, b_{1\ell}, \dots, b_{N\ell}, c_{1\ell}, \dots, c_{N\ell}, d_{1\ell}, \dots, d_{N\ell})^\top$$

is the $4N$ vector of unknowns. The system (7) leads to the following generalized eigenvalue problem:

$$\mathbf{L} \zeta = \sigma \operatorname{Gr} (\mathbf{Z}_1 \cos \beta + \mathbf{Z}_2 \sin \beta \cos \gamma) \zeta, \quad (8)$$

where $\mathbf{L}, \zeta, \mathbf{Z}_1$, and \mathbf{Z}_2 are block matrices given by

$$\mathbf{L} = \begin{pmatrix} \ddots & \vdots & \vdots & \vdots & \vdots \\ \cdots & -\mathbf{L}_{-1} & \epsilon \bar{\mathbf{V}} & \mathbf{O} & \cdots \\ \cdots & \epsilon \mathbf{V} & -\mathbf{L}_0 & \epsilon \bar{\mathbf{V}} & \cdots \\ \cdots & \mathbf{O} & \epsilon \mathbf{V} & -\mathbf{L}_1 & \cdots \\ \vdots & \vdots & \vdots & \vdots & \ddots \end{pmatrix},$$

$$\zeta = \begin{pmatrix} \vdots \\ \zeta_{-1} \\ \zeta_0 \\ \zeta_1 \\ \vdots \end{pmatrix}, \quad \mathbf{Z}_1 = \begin{pmatrix} \ddots & \vdots & \vdots & \vdots & \vdots \\ \cdots & \mathbf{U}_1 & \mathbf{O} & \mathbf{O} & \cdots \\ \cdots & \mathbf{O} & \mathbf{U}_1 & \mathbf{O} & \cdots \\ \cdots & \mathbf{O} & \mathbf{O} & \mathbf{U}_1 & \cdots \\ \vdots & \vdots & \vdots & \vdots & \ddots \end{pmatrix},$$

$$\mathbf{Z}_2 = \begin{pmatrix} \ddots & \vdots & \vdots & \vdots & \vdots \\ \cdots & \mathbf{U}_2 & \epsilon \bar{\mathbf{W}} & \mathbf{O} & \cdots \\ \cdots & \epsilon \mathbf{W} & \mathbf{U}_2 & \epsilon \bar{\mathbf{W}} & \cdots \\ \cdots & \mathbf{O} & \epsilon \mathbf{W} & \mathbf{U}_2 & \cdots \\ \vdots & \vdots & \vdots & \vdots & \ddots \end{pmatrix}.$$

We solve the generalized eigenvalue problem (8) numerically in order to obtain Gr as the real eigenvalue after feeding a trial value of k in the interval [0,8] for fixed values of the other parameters. The procedure is repeated for the other values of k . The critical Grashof number for the onset of the instability is then computed using the following formula:

$$\text{Gr}_c = \min_s \inf_{k, \gamma} \text{Gr}(\sigma, \epsilon, \omega, \beta, \gamma, s, k). \quad (9)$$

The critical wave number k_c is the value of k corresponding to Gr_c . We also define

$$\text{Gr}_c(\gamma) = \min_s \inf_k \text{Gr}(\sigma, \epsilon, \omega, \beta, \gamma, s, k). \quad (10)$$

The method described here resembles that of Kumar and Tuckerman [46], with a few exceptions. First, the solution in the present problem in the finite direction z is not available in closed form and must be approximated as a truncated series of Chandrasekhar functions. This makes the problem considerably more difficult and is an interesting generalization of the method of Kumar and Tuckerman [46]. Second, we have formulated the generalized eigenvalue problem (8) to choose the Grashof number as its eigenvalue instead of the amplitude of oscillation ϵ . This choice enables us to carry out effective numerical computations for obtaining marginal curves and hence the critical value of the control parameter. The present numerical method has been used in past research on temperature-modulated RBC in Refs. [34,35] and temperature-modulated VLC in Refs. [42,43].

For numerical computations, we have taken $0^\circ \leq \beta < 180^\circ$, $0^\circ \leq \gamma \leq 90^\circ$, $0 \leq \epsilon \leq 0.6$, and $0 < \omega \leq 200$. In this work, most of the numerical calculations have been performed for $\sigma = 0.71$ (air). The dependence of the onset and the nature of TMILC on σ are discussed separately.

IV. NUMERICAL RESULTS AND DISCUSSION

The two types of instability modes discussed in the present instability problem are (a) the temporal modes and (b) the spatial modes. The temporal modes are characterized by the forcing frequency ω . Floquet analysis computes the two temporal modes of the instability: the harmonic response in which the fluid layer oscillates time-periodically with the frequency ω , or the subharmonic response in which the fluid layer oscillates time-periodically with the frequency $\omega/2$. In a similar manner, the spatial modes are the orientations γ of a spatially

TABLE I. Comparison of the present numerical results with those obtained in Ref. [19] for the transverse mode of unmodulated ILC.

β	σ	Gr	Gr
		(Present)	Ref. [19]
0°	6.7	254.8898	254.9253
12°	6.7	278.3455	275.9701
24°	6.7	509.8482	500.0000
12°	0.71	2587.028	2569.014

periodic pattern of convective rolls in the xy -plane at the onset of TMILC. Among these orientations, the two most important spatial modes correspond to $\gamma = 0^\circ$ and 90° , which are called transverse and longitudinal modes, respectively.

Notation. Throughout, we shall denote by k_c^H and k_c^S the critical wave numbers corresponding to harmonic and subharmonic types of modes, respectively, in TMILC. We shall use the notation k_c^L and k_c^T for the wave numbers corresponding to longitudinal and transverse modes of the unmodulated ILC. Under modulation we shall denote by k_c^{LH} or k_c^{LS} the critical wave numbers for the longitudinal harmonic and subharmonic modes, respectively. Similarly, k_c^{TH} or k_c^{TS} will correspond to transverse harmonic or transverse subharmonic mode of TMILC. Finally, the symbol β_c will denote the value of β corresponding to the codimension-2 point in TMILC. Thus, for a given set of other parameter values, the preferred mode of the onset of TMILC is longitudinal for $\beta < \beta_c$ and transverse for $\beta > \beta_c$.

Equation (9) has been solved numerically with MATLAB in order to obtain the critical value of the control parameter for a given set of the other dimensionless parameters. To verify the correctness of the code, we have compared the numerical results obtained using the present scheme with those of Hart [19] in Table I for the unmodulated ILC for the Prandtl number of water and air. Clearly, the values of Gr as obtained using the present numerical method are in good agreement with the corresponding values given in Ref. [19]. The slight deviation in the numerical values of Gr might be due to finite aspect-ratio effects considered in Ref. [19]. Moreover, for $\epsilon = 0$ and $\sigma = 1.07$, the angle of inclination corresponding to the codimension-2 point has been found to occur for

$$(k_c^L, k_c^T, \text{Gr}_c) = (3.117875, 2.830625, 7526.231081),$$

where $\beta_c = 77.7567^\circ$ for $N = 10$, which is very close to the corresponding value $\beta_c = 77.7560^\circ$ as obtained recently in [21].

Finally, for $\epsilon > 0$, we have the following numerical values for $(\sigma, \beta) = (0.71, 90^\circ)$:

$$(\epsilon, \omega, k_c^H, k_c^S, \text{Gr}_c) = (0.3406, 5, 3.033, 2.648, 8561.187812)$$

for $N = 10$ and $L = 30$, which are in close agreement with the corresponding values obtained by Singh and Bajaj [42]. These observations verify the correctness of our numerical code.

After several numerical experiments, we have found that the present numerical scheme converges for $N \geq 10$ and $L \geq 20$, where for $\beta > 150^\circ$ larger values of $N \geq 15$ and

$L \geq 30$ are required to obtain numerical convergence. We have chosen N and L according to these constraints.

A. Marginal instability curves

For the Prandtl number of air ($\sigma = 0.71$), it is known that in the unmodulated ILC ($\epsilon = 0$), the critical value of the Grashof number corresponds to either a longitudinal mode ($\gamma = 90^\circ$) or a transverse mode ($\gamma = 0^\circ$), where the angle of inclination for the codimension-2 point is 71.4483° . So, the two most important configurations of ILC correspond to $\beta = 0^\circ$ and 90° .

Under modulation, for the case of temperature-modulated RBC ($\beta = 0^\circ$), Eq. (8) reduces to the eigenvalue problem

$$\mathbf{L}\zeta = \sigma \text{Gr} \mathbf{Z}_1 \zeta, \tag{11}$$

which is independent of γ . In this case, all spatial modes of the instability are equivalent. It is natural, of course, that the RBC solutions should be independent of γ , since homogeneous directions x and y are equivalent.

In contrast, in the case of VLC ($\beta = 90^\circ$), gravity is along the x direction, and so the x and y directions are not equivalent and γ is significant. For the temperature-modulated VLC, Eq. (8) yields the eigenvalue problem

$$\mathbf{L}\zeta = (\sigma \text{Gr} \cos \gamma) \mathbf{Z}_2 \zeta, \tag{12}$$

with eigenvalue $\sigma \text{Gr} \cos \gamma$ as a function of other parameters. So, in this case, Gr is proportional to $\sec \gamma$. Consequently, Gr_c corresponds to the minimum value of $\sec \gamma$ for $0^\circ \leq \gamma \leq 90^\circ$, which occurs for $\gamma = 0^\circ$. Thus, the onset of temperature-modulated VLC is always in the form of a transverse mode.

For the remaining configurations of the fluid layer, that is, for $0^\circ < \beta < 90^\circ$, the behavior of TMILC is not at all evident from Eq. (8). In view of this, we have obtained Fig. 2, which shows the variation of $\text{Gr}_c(\gamma)$ with γ for different values of β ; $\sigma = 0.71$, $\epsilon = 0.5$, and $\omega = 5$. The curves are labeled as H or S accordingly as $\text{Gr}_c(\gamma)$ corresponds to a harmonic or a subharmonic response. The curve $\beta = 80^\circ$ consists of two parts: a dashed subharmonic part for $0^\circ \leq \gamma \leq 58.02^\circ$ and a solid harmonic part for $58.02 \leq \gamma \leq 90^\circ$. For each of the curves in Fig. 2, the critical value Gr_c corresponds to the point marked \bullet . Clearly, for each value of β , the critical value of Gr corresponds to either $\gamma = 0^\circ$ or 90° . Here, the angle of inclination for the codimension-2 point is 64.806° . We conclude that under modulation, the onset of TMILC is either a longitudinal mode or a transverse mode. It can be observed from Fig. 2 that for $\beta = 90^\circ$, we have $\text{Gr}_c(\gamma) \rightarrow \infty$ as $\gamma \rightarrow 90^\circ$, which is in accordance with Eq. (12). This configuration ($\beta = 90^\circ$) of the fluid layer is stable with respect to all spatially longitudinal perturbations.

Figure 3 shows marginal curves in the (k, Gr) -plane for $\sigma = 0.71$, $\epsilon = 0.5$, and $\omega = 5$. Each subfigure in Fig. 3 has been obtained for one value of β . In each of the subfigures, the dashed curve in blue corresponds to the longitudinal harmonic (LH) mode. The thicker (red) and thinner (black) curves in each case correspond to the transverse harmonic (TH) and transverse subharmonic (TS) instability responses, respectively. The point marked \bullet on a particular marginal curve corresponds to the minimum for the particular type of instability mode. The marginal curve for $\beta = 0^\circ$ and $\epsilon = 0.5$ is

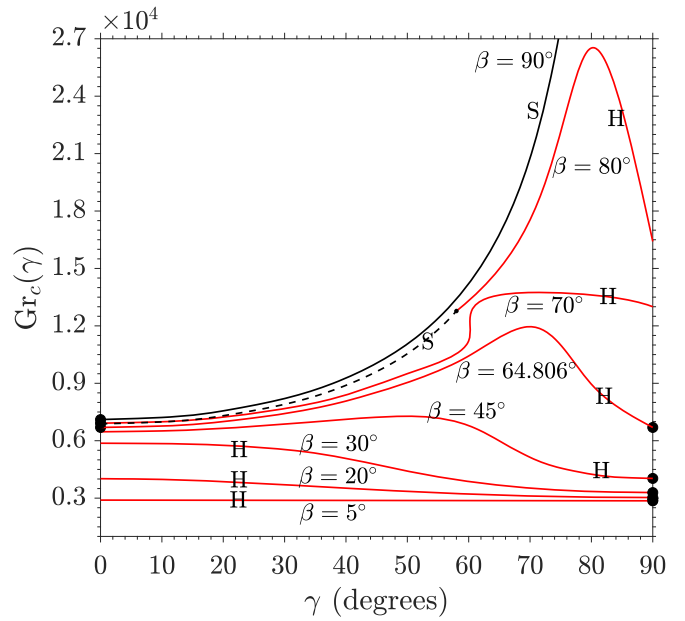


FIG. 2. $\text{Gr}_c(\gamma)$ vs γ for different values of β ; $\sigma = 0.71$, $\epsilon = 0.5$, and $\omega = 5$. Each point of minimum on a given curve is marked as \bullet . The curves are labeled as H and S to denote harmonic and subharmonic responses, respectively. The curve $\beta = 80^\circ$ consists of two parts: a dashed subharmonic branch and a solid harmonic branch.

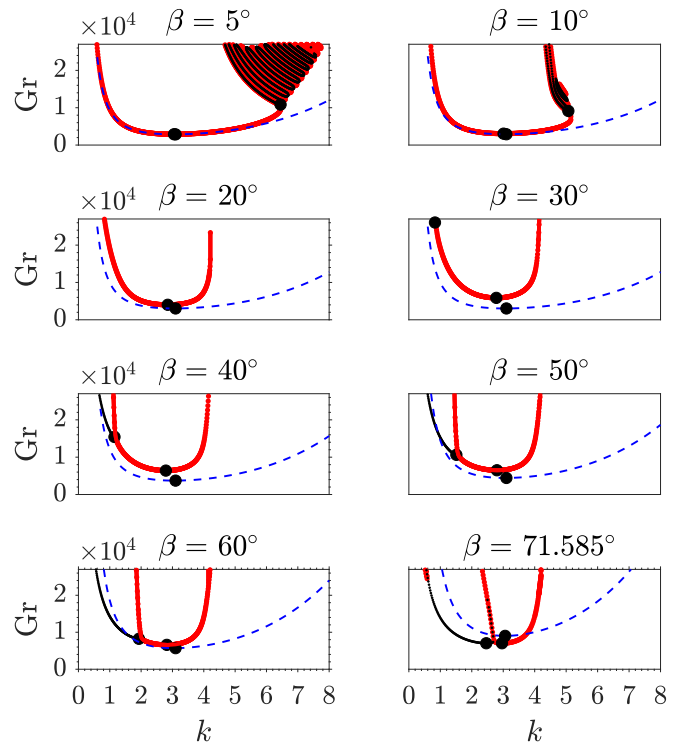


FIG. 3. The neutral instability curves in the (k, Gr) -plane for $\sigma = 0.71$, $\epsilon = 0.5$, and $\omega = 5$. The dashed (blue) curves correspond to LH mode. The thicker (red) and thinner (black) curves correspond to TH and TS instability responses, respectively. The point marked as \bullet in each case denotes the minimum for the particular type of instability mode.

known to consist of a single harmonic tongue (see Ref. [34]). However, even for the small value of $\beta = 5^\circ$, the marginal instability curves for the transverse mode consist of alternate harmonic and subharmonic tongues, where a comparatively wide harmonic instability tongue is followed by a narrow pattern of alternate subharmonic and harmonic closed curves. The basic flow is unstable with respect to any type of perturbations for the points within a particular closed curve (island), and stable for the points outside it. It is interesting to note that the marginal curves in the form of isolated closed islands are found to occur in the Faraday instability under two-frequency modulation as obtained in Ref. [27]. The lowest value of Gr for the transverse mode occurs on the wider harmonic branch of the marginal curves. On the other hand, the marginal curve for the longitudinal mode consists of a single wide harmonic tongue (here, only the lower part of the marginal curve is shown for the LH mode) on which Gr_c is attained and no subharmonic response is found to occur for $(\epsilon, \omega) = (0.5, 5)$. This can be explained from the analysis of the underlying perturbation equations. For the longitudinal roll solution for TMILC, we have $\frac{\partial}{\partial x} \equiv 0$ or equivalently $\gamma = 90^\circ$. In view of this, (5a) and (5b) reduce to the following:

$$\frac{1}{\sigma} \frac{\partial \nabla^2 w}{\partial t} = \nabla^4 w + \sigma Gr \cos \beta \frac{\partial^2 \theta}{\partial y^2}, \quad (13a)$$

$$\frac{\partial \theta}{\partial t} + w \frac{\partial T_e}{\partial z} = \nabla^2 \theta, \quad (13b)$$

$$\left(w, \frac{\partial w}{\partial z}, \theta \right) \Big|_{z=\pm \frac{1}{2}} = (0, 0, 0). \quad (13c)$$

Note that the perturbation equations (13a)–(13c) are essentially those that were obtained for the problem of temperature-modulated RBC in Ref. [33] in the absence of magnetic field and in Ref. [34] except that $\sigma Gr \cos \beta$ appears in (13a) in place of σGr . So, the nature of the onset of the instability in TMILC in the form of a longitudinal mode for any inclination β can be expressed in terms of the control parameter and the wave number for temperature-modulated RBC, that is,

$$Gr|_{0^\circ \leq \beta < 90^\circ} = Gr|_{\beta=0^\circ} \times \sec \beta, \quad \gamma = 90^\circ, \quad (14a)$$

$$k|_{0^\circ \leq \beta < 90^\circ} = k|_{\beta=0^\circ}, \quad \gamma = 90^\circ. \quad (14b)$$

We find that (14a) and (14b) in particular recover the result of Greshuni and Zhukhovitskii [47] corresponding to the unmodulated ILC. Since subharmonic marginal curves do not appear in temperature-modulated RBC [34] for $\epsilon = 0.5$ and $\omega = 5$ in the considered range of the control parameter, the same must be true for TMILC for $\gamma = 90^\circ$ in Fig. 3.

Returning to Fig. 3, we observe that for $\beta = 5^\circ$, the critical value of the control parameter for TMILC corresponds to a longitudinal-harmonic (LH) mode. The pattern of closed TH and TS curves appears for up to $\beta = 10^\circ$, where the number of such closed marginal curves decreases on incrementing β . The leftmost wide TH marginal curve becomes narrower on increasing β . The closed marginal curves do not appear for $10^\circ < \beta \leq 90^\circ$ in the considered range of Gr. For

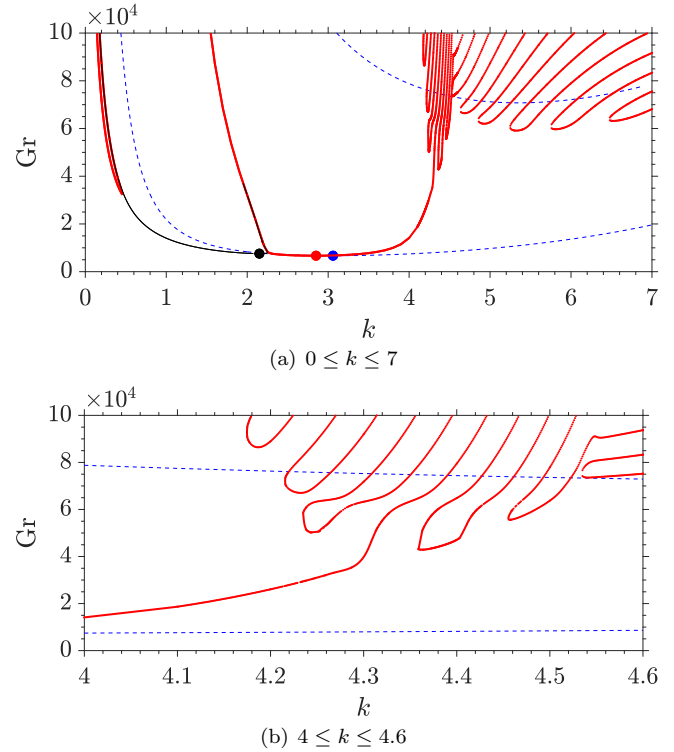


FIG. 4. Neutral instability curve in the (k, Gr) -plane for $\beta = 64.806^\circ$. The other parameter values are the same as in Fig. 3. The black, red, and blue solid circles denote the minimum for TS, TH, and LH responses respectively.

$\beta = 30^\circ$, a small TS branch appears to the left of the wider TH branch of the marginal curves. The entire pattern of TH, TS, and LH marginal curves shifts upwards in the (k, Gr) -plane on incrementing β from 0° to 90° , which indicates that in TMILC, the critical Grashof number increases with increasing β . This is natural since an increase in the inclination of the layer causes an increase in the flow shear, which stabilizes the basic flow field, and so a larger temperature gradient is required in order to observe TMILC. The critical mode for the onset of TMILC remains LH for $0^\circ \leq \beta \leq 64.806^\circ$, where the angle of inclination $\beta = \beta_c$ denotes the codimension-2 point for mode switching between longitudinal and transverse types with the following critical values:

$$(\beta_c, k_c^{LH}, k_c^{TH}, Gr_c) = (64.806^\circ, 3.0578, 2.8475, 6693.30).$$

We provide a more detailed description of the marginal curves for $\beta_c = 64.806$ separately in Fig. 4(a).

A meandering pattern of marginal curve is observed in a neighborhood of $k = 4.1$ as shown in Fig. 4(b). This meandering pattern is found to be a characteristic of marginal curves not only for $\beta = \beta_c$ but also for all other positive inclinations. Furthermore, the marginal curves for TH or LH responses are found to occur for larger wave numbers, whereas TS response is not observed to occur for large wave numbers in the considered limits of Gr.

Returning to Fig. 3, we find that for $\beta \geq \beta_c$, the critical Grashof number always corresponds to a TH or a TS mode. On further incrementing β , a bicritical point is observed to

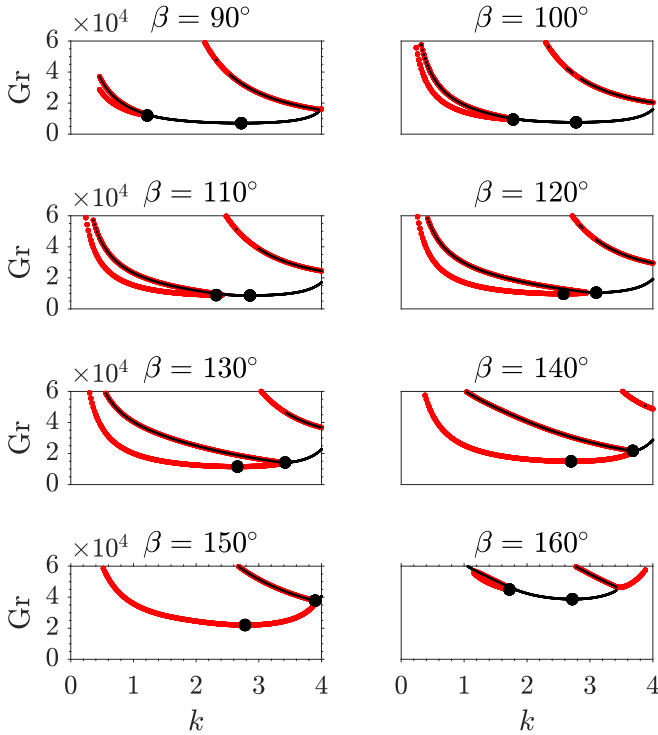


FIG. 5. The neutral instability curves in the (k, Gr) -plane for the fixed parametric values and other parameters as in Fig. 3.

occur for $\beta \approx 71.585^\circ$ with

$$(k_c^{TH}, k_c^{TS}, Gr_c) = (2.9675, 2.4675, 7025.85).$$

The instability tongues corresponding to this bicritical point are of comparable sizes. For $\beta = 80^\circ$ (the graph not shown here), the critical mode of instability is in the form of a pattern of transverse convective rolls executing subharmonic oscillations.

The marginal instability curves for $\beta \geq 90^\circ$ have been shown in Fig. 5 for the fixed parametric values as in Fig. 3. For $90^\circ \leq \beta < 180^\circ$ and $\epsilon = 0.5$, the longitudinal mode has not been found to occur in TMILC. This is natural since for β in the range from 90° to 180° , the upper plane bounding the layer is hotter than the lower one, which causes the modulation effects to act against buoyancy effects, whereas the longitudinal mode of the instability is buoyancy-dominated. Consequently, the instability response is either TH or TS, depending upon β . The lowest value of Grashof number occurs on the middle subharmonic marginal curve for $\beta = 90^\circ, 100^\circ$, and 110° . In each of these cases, the marginal curves alternate between the middle subharmonic branch accompanied by two left and right harmonic branches. The leftmost harmonic branch is narrow but widens as β is incremented, and for $\beta = 120^\circ$, Gr_c occurs on the leftmost harmonic marginal curve in the (k, Gr) -plane. For $\beta = 120^\circ, 140^\circ$, and 150° , the instability response remains harmonic, whereas for $\beta = 160^\circ$, the lowest value of Gr occurs on the middle subharmonic branch. A switching between the two temporal modes occurs through an intermediate bicritical state in which the fluid layer oscillates time-periodically with the coexistence of two distinct wave numbers. For $\beta = 180^\circ$, we are back at the case of RBC, but

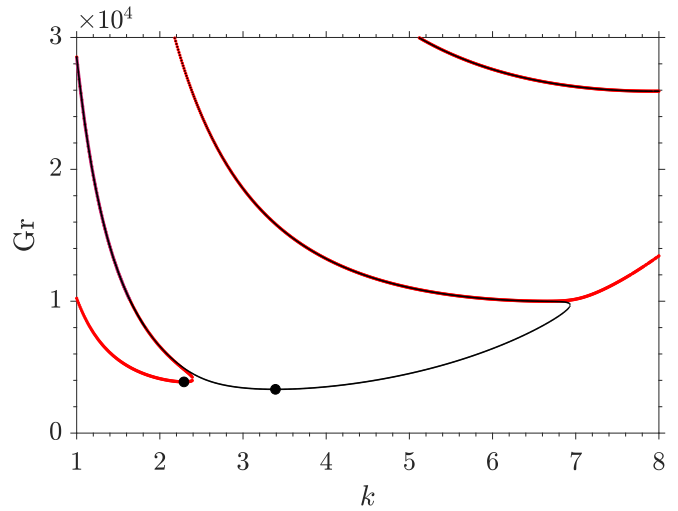


FIG. 6. Neutral instability curve in the (k, Gr) -plane for $\sigma = 0.71$, $\epsilon = 0.6$, $\omega = 5$, $\gamma = 90^\circ$, and $\beta = 0^\circ$. Each \bullet denotes the minimum for LH or LS response.

in the stable configuration (the upper plane hotter than the lower colder plane). Two bicritical points are found to occur for $\beta \approx 112.63^\circ$ and 153.047° , and the details are given in Fig. 8.

We have obtained marginal curves for a slightly larger value of $\epsilon = 0.6$ in Fig. 6 for $\sigma = 0.71$, $\omega = 5$, $\gamma = 90^\circ$, $\beta = 0^\circ$. Here, the instability sets in first as a LS mode with the following critical values:

$$(k_c^{LS}, Gr_c) = (3.3916, 3319.02).$$

Consequently using (14a) and (14b), the onset of the instability in TMILC for the Prandtl number of air remains in the form of a LS mode for $0^\circ < \beta < \beta_c$ for $\epsilon = 0.6$ and $\omega = 5$.

We conclude that the onset of TMILC is one of LS or LH modes for $0^\circ < \beta < \beta_c$, depending upon the modulation parameters.

Under high-frequency modulation and small inclinations of the fluid layer, we have observed a beautiful ‘‘Boot-pattern’’ of the marginal curves corresponding to the transverse mode. Figure 7 shows such a pattern for the Prandtl number of air, $\epsilon = 0.5$ and $\omega = 50$. It is known that for $\beta = 0^\circ$, the case of RBC, there is a single wide TH instability tongue in the (k, Gr) -plane within which the basic flow is unstable and stable otherwise [42].

For the parts of Fig. 7 corresponding to $\beta = 1^\circ$, multiple (disjoint) marginal curves alternate between harmonic and subharmonic branches. The largest and leftmost branch is a boot-shaped harmonic branch, and Gr_c occurs on this marginal curve. The leftmost largest harmonic branch is followed by alternate disjoint subharmonic and harmonic small closed curves, as is more evident from the subfigures corresponding to $\beta = 2^\circ - 5^\circ$. The entire pattern shifts towards lower wave-numbers on incrementing β . For $\beta = 7^\circ$, a single larger leftmost harmonic instability tongue appears along with multiple smaller marginal curves alternating between harmonic and subharmonic types and also a pattern of closed curves alternating between harmonic and subharmonic types. With a further increase of β , the

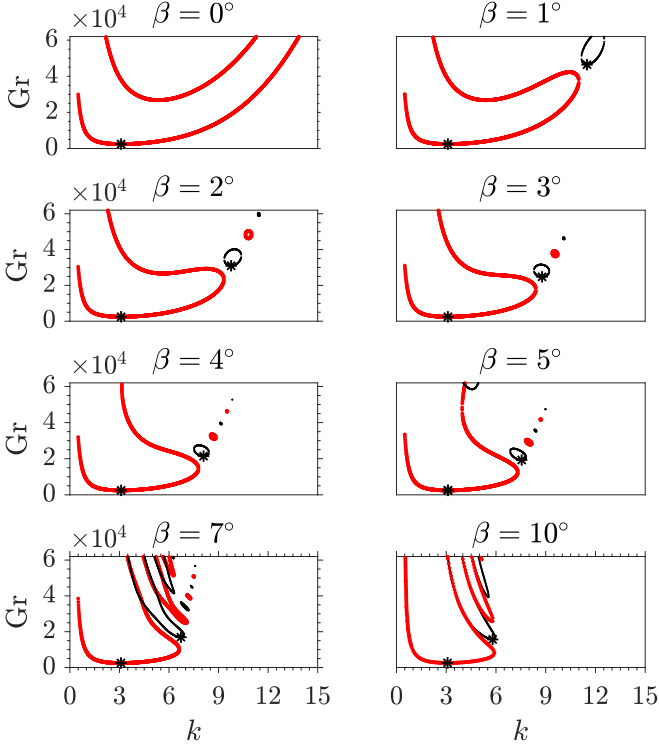


FIG. 7. Marginal curve in the (k, Gr) -plane for the transverse mode of TMILC for $\sigma = 0.71$, $\epsilon = 0.5$, and $\omega = 50$. The thicker (red) and thinner (black) parts of the curve correspond to TH and TS responses, respectively. Each of the points marked * denotes a minimum for the underlying temporal mode.

entire pattern of the smaller instability tongues and the closed loops come closer, and eventually merge together for $\beta \approx 10^\circ$. Marginal curves exhibiting a pattern alternating between subharmonic and harmonic “islands” have not been reported in any Floquet problem in the past, although “islands” have been found to occur in the marginal curves for two-frequency excitation of Faraday instability in Ref. [27].

B. Effect of angle of inclination on critical values of Gr and k

Figure 8 shows the variation of Gr_c with β for $\sigma = 0.71$, $\epsilon = 0, 0.5$, and $\omega = 5$. For the unmodulated ILC, that is, for $\epsilon = 0$, the instability response is a longitudinal mode for β in the range 0° – 71.44° , whereas the instability response is a transverse mode for $71.44^\circ < \beta < 180^\circ$. In addition, Gr_c is an increasing function of β , where $Gr_c \rightarrow \infty$ as $\beta \rightarrow 180^\circ$. This is due to the fact that $\beta = 180^\circ$ is the stable RBC configuration of the fluid layer heated from above and cooled from below.

A similar variation of Gr_c with β is found to occur under modulation for $\epsilon = 0.5$ and $\omega = 5$. Here, the preferred mode for the onset of TMILC is a LH mode for $0^\circ \leq \beta < 64.806^\circ$. The angle of inclination 64.806° corresponds to the codimension-2 point (also see Fig. 4). For $64.806^\circ < \beta < 71.585^\circ$, the instability response is a TH mode, and a bicritical point is observed to occur for $\beta \approx 71.585^\circ$ with the following critical values:

$$(k_c^{\text{TH}}, k_c^{\text{TS}}, Gr_c) = (2.9675, 2.4675, 7025.846).$$

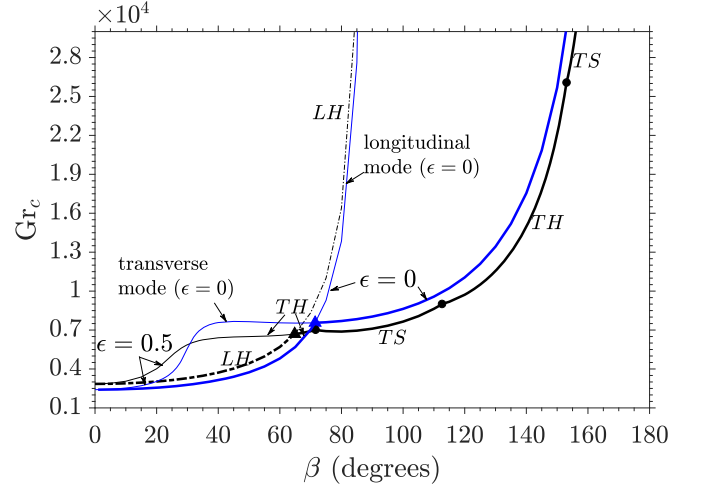


FIG. 8. Gr_c vs β for $\sigma = 0.71$, $\epsilon = 0, 0.5$, and $\omega = 5$. The blue and black curves correspond to $\epsilon = 0$ and 0.5 , respectively. The thicker curves correspond to (k_c, Gr_c) for the most unstable mode for a given value of ϵ and β . For $\epsilon = 0.5$, the critical curve consists of LH, TS, TH, and TS parts separated by a bicritical point marked as \bullet . The points marked \blacktriangle on curves $\epsilon = 0$ and 0.5 correspond to β_c .

For $71.585^\circ < \beta < 112.63^\circ$, the instability response in TMILC is a TS mode until another bicritical point occurs for

$$(\beta, k_c^{\text{TS}}, k_c^{\text{TH}}, Gr_c) = (112.63^\circ, 2.9143, 2.4300, 9011.171).$$

For $112.63^\circ < \beta < 153.047^\circ$, the instability response is a TH mode. Yet another bicritical point is found to occur for $\beta \approx 153.047^\circ$ with

$$(k_c^{\text{TH}}, k_c^{\text{TS}}, Gr_c) = (2.9060, 2.4690, 26076.20).$$

Beyond $\beta = 153.047^\circ$, the instability response is found to be a TS mode. It is interesting to observe that

$$Gr_c|_{\epsilon=0} \begin{cases} < Gr_c|_{\epsilon=0.5} \text{ for } 0^\circ \leq \beta < 70^\circ, \\ > Gr_c|_{\epsilon=0.5} \text{ for } 70^\circ < \beta < 180^\circ. \end{cases}$$

This shows that the onset of TMILC gets delayed by modulation for $0^\circ \leq \beta < 71.585^\circ$, which is in accordance with (14a), and the onset gets advanced under modulation for $71.585^\circ < \beta < 180^\circ$.

The corresponding variation of k_c with β is shown in Fig. 9. The critical wave-number k_c^{L} or k_c^{LH} for the onset of TMILC is independent of β in the absence as well as the presence of the modulation, which is in accordance with (14b). However, the critical wave-number corresponding to the transverse mode depends strongly on β . For $\epsilon = 0$, k_c^{T} is a decreasing continuous function of β up to approximately 168° , beyond which k_c^{T} increases sharply with β on further increase of β . Under modulation, k_c is discontinuous at the value β_c at which the bicritical point occurs in TMILC. The mode switches at a bicritical point between harmonic and subharmonic types. Between any two consecutive bicritical points, k_c is an increasing function of β .

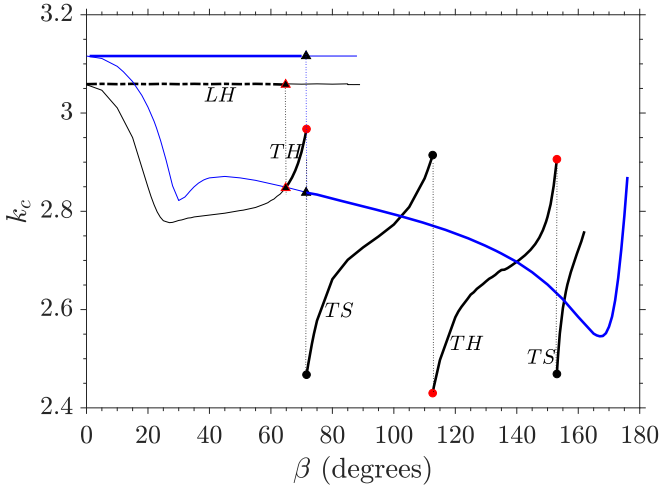


FIG. 9. k_c vs β for the same parameter values and other details as in Fig. 8.

C. Effect of modulation on mode switching

The angle of inclination for the codimension-2 point in the steady ILC is $\beta_c \approx 71.4483^\circ$ for the Prandtl number of air, with the following critical values:

$$(k_c^L, k_c^T, Gr_c) \approx (3.116, 2.838, 7560.02199).$$

Under modulation, the parameter β_c is a function of the modulation parameters. In view of this, we have obtained Fig. 10, which shows the variation of β_c with ϵ for $\sigma = 0.71$, and for $\omega = 5, 10$. The solid (red), solid (black), and dashed (black) parts of the curve correspond to TH-LH, TS-LH, and TH-LS modes, respectively. Each of the points marked \bullet corresponds to a bicritical point.

First we explain the curve $\omega = 5$. The parameter β_c decreases slightly from 71.4483° to 71.03° , when ϵ is varied from 0 to approximately 0.3, where the instability response of TMILC is harmonic. For $0.3 \leq \epsilon \leq 0.3428$, the parameter β_c increases slightly with ϵ , and a bicritical point is observed

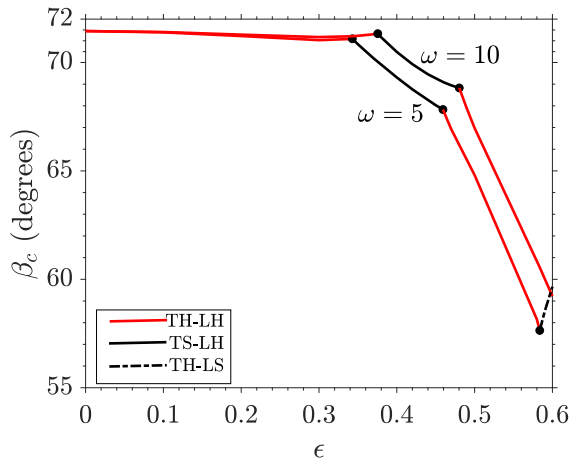


FIG. 10. β_c vs ϵ for $\sigma = 0.71$ and $\omega = 5, 10$. The solid (red), solid (black), and dashed (black) parts of each curve correspond to TH-LH, TS-LH, and TH-LS modes, respectively. Each of the points marked \bullet corresponds to a bicritical point.

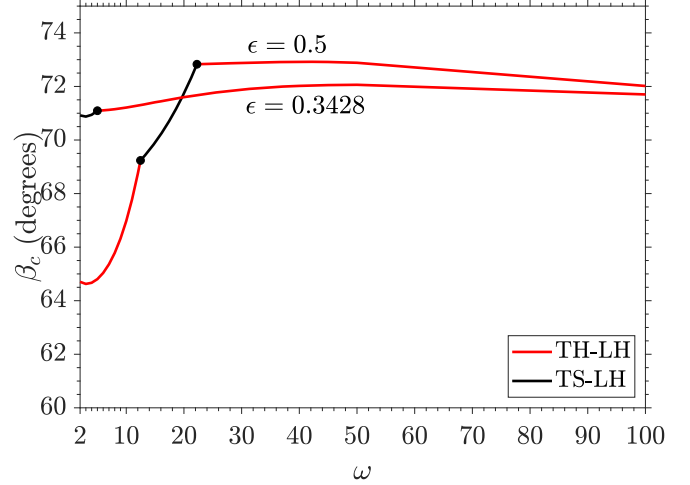


FIG. 11. β_c vs ω for $\sigma = 0.71$ and $\epsilon = 0.5, 0.3428$. The red and black parts of the curve correspond to TH-LH and TS-LH responses, respectively. Each of the points marked \bullet corresponds to a bicritical point.

to occur for $\epsilon \approx 0.3428$ and $\beta_c = 71.094^\circ$ with the following critical values:

$$(k_c^{TH}, k_c^{TS}, k_c^{LH}, Gr_c) \approx (3.019, 2.579, 3.104, 7903.3).$$

For $0.3428 < \epsilon < 0.4593$, the instability response is subharmonic and β_c decreases significantly to 67.83° for $\epsilon = 0.4528$ when another bicritical point occurs for the following critical values:

$$(k_c^{TS}, k_c^{TH}, k_c^{LH}, Gr_c) \approx (2.486, 2.980, 3.081, 7264.6).$$

Beyond $\epsilon = 0.4593$, β_c decreases rapidly with ϵ and the instability response remains harmonic for $0.4593 < \epsilon < 0.5837$. For $\epsilon \approx 0.5837$, a bicritical point is found to occur for $\beta_c \approx 57.642$ with the following critical values:

$$(k_c^{TH}, k_c^{LH}, k_c^{LS}, Gr_c) \approx (2.663, 2.617, 3.567, 6478.6).$$

For $0.5837 < \epsilon \leq 0.6$, the instability response is subharmonic. These observations show that under modulation, the inclination corresponding to the codimension-2 point is either harmonic, or subharmonic, or bicritical, depending upon the amplitude of modulation. A similar variation of β_c with ϵ occurs for $\omega = 10$ with a difference that the TH-LS mode is not found to occur for the considered range of ϵ . Further, for $\omega = 10$, the instability region for the onset of the longitudinal mode expands in comparison with that for $\omega = 5$.

To see the dependence of β_c on ω , we have obtained Fig. 11 for two distinct values of $\epsilon = 0.3428, 0.5$ and $\sigma = 0.71$. The red and black parts of each of the curves in Fig. 11 correspond to harmonic and subharmonic responses, respectively. It is evident from Fig. 11 that the locus of the angle of inclination corresponding to the codimension-2 point in the (ω, Gr_c) -plane for TMILC consists of alternating TH-LH and TS-LH branches connected through an intermediate bicritical point. First we explain the curve $\epsilon = 0.3428$. For $2 \leq \omega < 5$, the codimension-2 point occurs through a TS-LH response, where β_c decreases with ω for $2 \leq \omega < 4$, attains a minimum for $\omega \approx 4$, and increases with ω for $4 < \omega < 5$. For $\omega = 5$, the codimension-2 point corresponds to a bicritical point as

discussed earlier for $\beta_c \approx 71.094^\circ$. For $\omega > 5$, the value of β_c corresponds to a TH-LH response, where β_c increases with ω for $5 < \omega < 50$ and attains a maximum value $\beta_c \approx 72.0620^\circ$ for $\omega \approx 50$. Only 1.36% increase in β_c with ω is observed to occur for $\omega > 5$, which shows that in TMILC, high-frequency modulation will have little effect on the angle of inclination corresponding to the codimension-2 point. Beyond $\omega = 50$, β_c decreases slowly with a further increase of ω and eventually approaches the following:

$$\lim_{\omega \rightarrow \infty} \beta_c(\omega) = 71.4483^\circ = \lim_{\epsilon \rightarrow 0} \beta_c. \quad (15)$$

A similar dependence of β_c on ω can be observed for $\epsilon = 0.5$, where the dependence is significant for $2 \leq \omega \leq 22.254$. Here, β_c corresponds to a TH-LH response for $2 \leq \omega < 12.469$, and a bicritical point is observed for $\omega \approx 12.469$, where $\beta_c \approx 69.237^\circ$ corresponding to the following numerical values:

$$(k_c^{\text{TH}}, k_c^{\text{TS}}, k_c^{\text{LH}}, \text{Gr}_c) = (3.018, 2.239, 3.071, 7715.8).$$

For $\epsilon = 0.5$, the parameter β_c decreases with ω for $2 \leq \omega \leq 3$, attains a minimum for $\omega = 3$, and then β_c increases rapidly with ω for $3 \leq \omega \leq 22.254$. For $12.469 < \omega < 22.254$, β_c corresponds to a TS-LH response, when another bicritical point occurs for $\omega \approx 22.254$ and $\beta_c \approx 72.829^\circ$, which correspond to the following values:

$$(k_c^{\text{TS}}, k_c^{\text{TH}}, k_c^{\text{LH}}, \text{Gr}_c) = (2.023, 3.009, 3.081, 8837.8).$$

Beyond $\omega = 22.254$, the variation in β_c with ω for $\epsilon = 0.5$ is similar to that in the case of $\epsilon = 0.3428$.

D. Flow field and isotherms

For computing the projection of the flow field in the (x, z) -plane, it is necessary to compute the velocity components u and w at each point (x, z) for a given value of t and y . For longitudinal as well as transverse modes, the component w is given by (6a). For the transverse mode, u can be calculated in terms of w from the equation of continuity.

On the other hand, for the longitudinal mode, the velocity component u can be computed as a function of w and θ as follows. First, we observe that the momentum balance along the x -direction gives

$$\begin{aligned} \frac{1}{\sigma} \frac{\partial u}{\partial t} + \text{Gr} \sin \beta \left(\frac{\partial V_e}{\partial z} w + V_e \frac{\partial u}{\partial x} \right) \\ = -\frac{1}{\sigma} \frac{\partial p}{\partial x} + \nabla^2 u + (\sigma \text{Gr} \sin \beta) \theta. \end{aligned} \quad (16)$$

For the longitudinal mode, we have $\partial/\partial x \equiv 0$. This in view of (16) gives

$$\left(\nabla^2 - \frac{1}{\sigma} \frac{\partial}{\partial t} \right) u = \text{Gr} \sin \beta \left(w \frac{\partial V_e}{\partial z} - \sigma \theta \right), \quad (17)$$

along with the boundary conditions $u|_{z=\pm 1/2} = 0$. Thus the preceding two-point boundary value problem can be solved for u in terms of the solutions for w and θ .

Figure 12 shows the stream function for the disturbances in the velocity field of the perturbed flow and the isolines for the disturbance θ in the temperature field, each normalized to unity in (a) (y, z) -plane for LH mode, and (b)

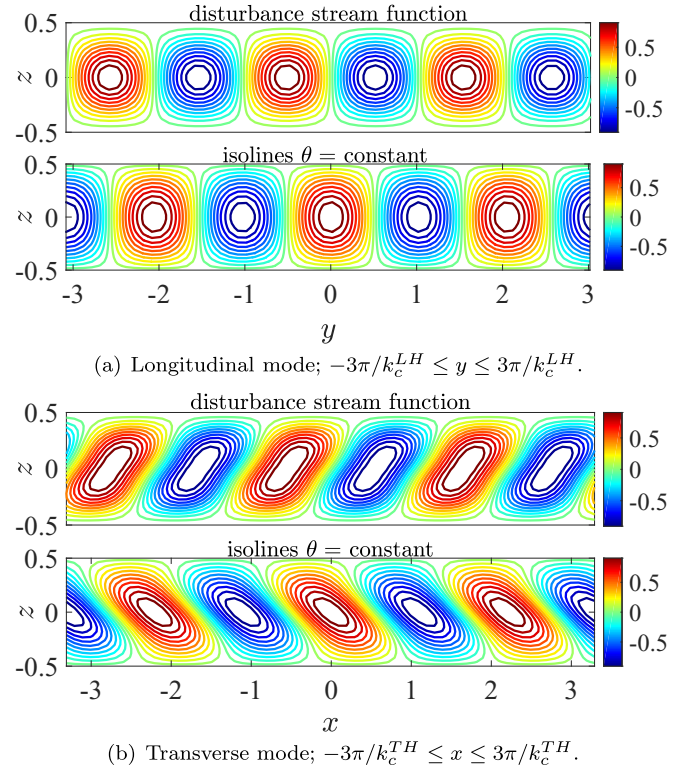
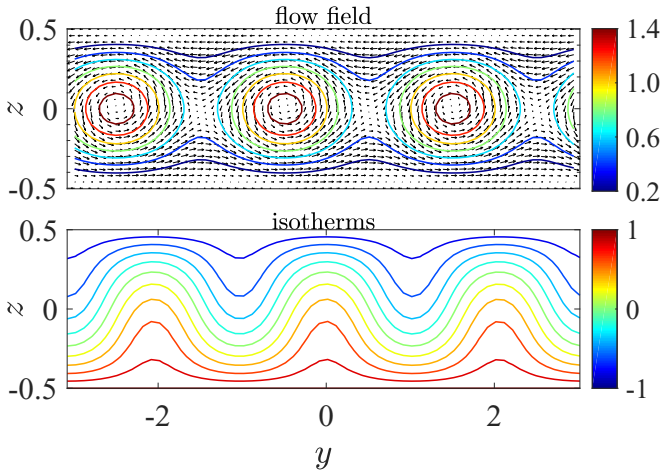


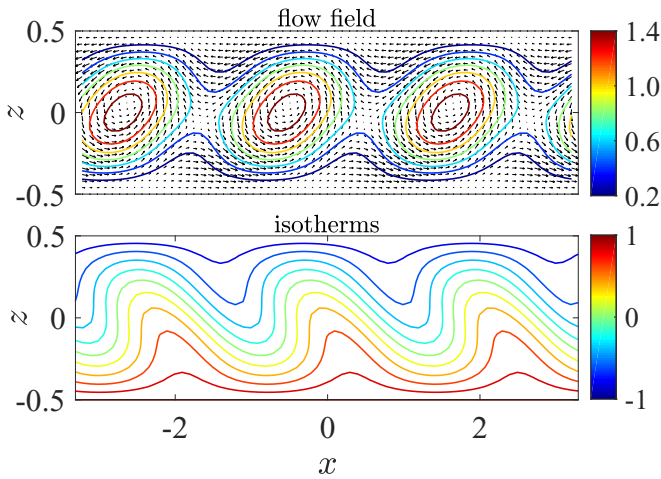
FIG. 12. Normalized disturbance stream function, and isolines for normalized θ for $\beta = 64.806^\circ$, $\epsilon = 0.5$, $\omega = 5$, $\sigma = 0.71$, and $t = 0.2513$ in (a) (y, z) -plane for LH mode, and (b) (x, z) -plane for TH mode, at the onset of TMILC.

(x, z) -plane for TH mode, at the onset of TMILC, for the inclination corresponding to the codimension-2 point, that is, $\beta = 64.806^\circ$; $\epsilon = 0.5$, $\omega = 5$, $\sigma = 0.71$, and $t = 0.2513$. We observe from the first subfigure of Fig. 12(a) that the longitudinal perturbations manifest themselves in the form of an alternating periodic pattern of identical cells extending along the y direction. The flow-field perturbations in adjacent cells have opposite orientations, and the boundary separating them corresponds to the location where the temperature perturbation has the highest magnitude. The pattern of the isolines $\theta = \text{const}$ is similar, as can be seen from the second subfigure in Fig. 12(a). On the other hand, the corresponding pattern of the disturbance stream function corresponding to the perturbations (u, w) and the isolines for θ in the case of TS mode is shown in Fig. 12(b), where we observe that the transverse disturbances in the flow field manifest themselves in the form of an alternating periodic pattern of identical tilted cells extending along the x direction. A similar pattern for the isolines $\theta = \text{const}$ can be seen from the second subfigure of Fig. 12(b).

Finally, for a given mode, the total flow field has been taken to be $(V_e + \delta \times v, w)$ for the LH mode and $(V_e + \delta \times v, w)$ for the TH mode, where each of V_e , u , v , and w has been normalized to 1, and δ with $0 < \delta < 1$ is used to scale the perturbation in the basic flow field. Similarly, the temperature field has been taken to be $T_e + \delta \times \theta$, where T_e and θ are normalized to 1. The pattern of the flow field (upper subfigure) and the isotherms (lower subfigure) has been shown for the LH mode in Fig. 13(a) in the (y, z) -plane, and for the TH



(a) Longitudinal mode; $-3\pi/k_c^{LH} \leq x \leq 3\pi/k_c^{LH}$.



(b) Transverse mode; $-3\pi/k_c^{TH} \leq x \leq 3\pi/k_c^{TH}$.

FIG. 13. Velocity vector field and isotherms for $\beta = 64.806^\circ$, $\delta = 0.5$, $\epsilon = 0.5$, $\omega = 5$, and $\sigma = 0.71$ for $t = 0.2513$ in (a) the (y, z) -plane for LH mode, (b) the (x, z) -plane for TH mode.

mode in Fig. 13(b) in the (x, z) -plane at the onset of TMILC for $\beta = 64.806^\circ$, $\delta = 0.5$, $\epsilon = 0.5$, $\omega = 5$, and $\sigma = 0.71$ for $t = 2\pi/(5\omega)$ and $y = 0$. The vector plot in the first subfigure of each of Figs. 13(a) and 13(b) shows the direction of the velocity vector field. We observe that the flow in each case (LH or TH) is up the slope in the hotter part of the fluid layer, and the flow is down the slope in the cooler part of the fluid layer. The longitudinal rolls have their axis parallel to the x -axis. On the other hand, the transverse rolls have their axis parallel to the y -axis. So, the transverse rolls are visible in the (x, z) -plane where the flow is identical within adjacent rolls. Further, we observe that as expected, the longitudinal-roll pattern as in Fig. 13(a) is identical to that of the RBC but with a difference that in RBC, the flow alternates between clockwise and anticlockwise within adjacent rolls, whereas the flow within adjacent rolls is identical in the longitudinal-roll pattern for $\beta = 64.806^\circ$. On the other hand, the transverse-roll pattern in Fig. 13(b) is identical to that of VLC. We have observed that in each case (LH or TH), the pattern of the flow field remains almost the same as shown in Fig. 13 for all values of t , however movements of the isotherms for the

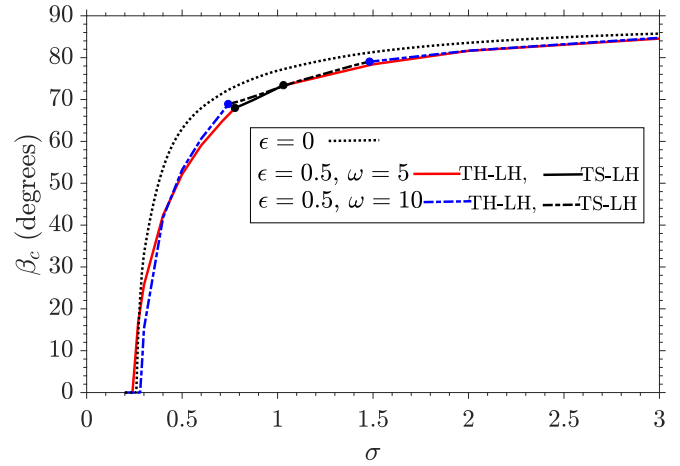


FIG. 14. β_c vs σ for $\epsilon = 0, 0.5$ and $\omega = 5, 10$. The dotted curve corresponds to $\epsilon = 0$. The solid red and black parts on the curve $(\epsilon, \omega) = (0.5, 5)$ correspond to TH-LH and TS-LH responses, respectively. Similarly, the dashed-dotted blue and black parts on the curve $(\epsilon, \omega) = (0.5, 10)$ correspond to TH-LH and TS-LH responses, respectively. Each of the points marked \bullet corresponds to a bicritical point.

total temperature field in the layer are observed to occur over a time period, which allows a time-periodic heat transfer from the hotter boundary to the cooler boundary of the layer.

V. PRANDTL NUMBER DEPENDENCE

Figure 14 shows the variation of β_c with σ for $\epsilon = 0, 0.5$ and $\omega = 5, 10$. The dotted, solid, and dashed-dotted curves correspond to $\epsilon = 0$, $(\epsilon, \omega) = (0.5, 5)$, and $(\epsilon, \omega) = (0.5, 10)$, respectively.

The solid red and black parts on the curve $(\epsilon, \omega) = (0.5, 5)$ correspond to TH-LH and TS-LH responses, respectively. Similarly, the dashed-dotted blue and black parts on the curve $(\epsilon, \omega) = (0.5, 10)$ correspond to TH-LH and TS-LH responses, respectively. In the absence of modulation ($\epsilon = 0$), the parameter β_c is a monotonically increasing function of σ , where the rate of increase of β_c with respect to σ is sharp for small values of σ and the rate is negligible for large values of σ . It is well known that for the unmodulated ILC, $\beta_c = 0^\circ$ for all fluids with $\sigma < 0.26$ and $\beta_c > 0$ for $\sigma \geq 0.26$ approximately [48,49]. This can be explained as follows. For the fluids with small Prandtl number, the kinetic energy of the mean flow is larger than the potential energy associated with the density stratification, and the transverse perturbations receive energy from the mean flow, thereby leading to a hydrodynamic origin of the instability in the form of transverse modes for all angles of inclinations [48].

Under modulation ($\epsilon = 0.5$), a similar observation prevails. In fact, the variation of β_c with σ is similar in the two typical cases $\epsilon = 0$ and 0.5 except that for $\epsilon = 0.5$, the nature of the onset of the instability for β_c can be one of the three modes TH-LH, TS-LH, and TH-TS-LH. More precisely, for $\epsilon = 0.5$ and $\omega = 5$, $\beta_c > 0^\circ$ for all $\sigma \geq 0.24$ and $\beta_c = 0^\circ$ otherwise. In addition, β_c corresponds to the TH-LH mode for $0 < \sigma < 0.7766$ and a bicritical point (a TH-TS-LH mode)

with $(\sigma, \beta_c) \approx (0.7766, 67.996^\circ)$ and the following critical values:

$$(k_c^{\text{TH}}, k_c^{\text{TS}}, k_c^{\text{LH}}, \text{Gr}_c) \approx (2.971, 2.492, 3.051, 6921.34).$$

For $0.7766 < \sigma < 1.0308$, the parameter β_c corresponds to a TS-LH mode. The value $\sigma = 1.0308$ corresponds to another bicritical point with $\beta_c \approx 73.4314^\circ$ and the following critical values:

$$(k_c^{\text{TS}}, k_c^{\text{TH}}, k_c^{\text{LH}}, \text{Gr}_c) \approx (2.900, 2.478, 3.038, 6719.5).$$

For $\sigma > 1.0308$, β_c corresponds to a TH-LH mode, where for all sufficiently large values of σ , the rate of change of β_c with σ is negligible.

A similar variation of β_c with σ occurs for $\epsilon = 0.5$ and $\omega = 10$ (dashed-dotted curves), where we note that $\beta_c = 0^\circ$ for $\sigma < 0.279$ and $\beta_c > 0^\circ$ otherwise. Furthermore, β_c corresponds to a TH-LH mode for $0 < \sigma < 0.7414$, a TS-LH mode for $0.7414 < \sigma < 1.4815$, and a TH-TS-LH mode for $\sigma = 0.7414, 1.4815$. The curves $\omega = 5$ and 10 are practically indistinguishable for $\sigma > 1$, which indicates that under modulation, an increase of ω has a negligible effect on β_c for high Prandtl number fluids.

VI. CONCLUDING REMARKS

Floquet analysis of TMILC reveals interesting features about the nature of the onset of instability. The marginal instability curves (and hence the type of instability response) for the longitudinal perturbations in TMILC are completely determined from those that exist in the temperature-modulated RBC for the corresponding parametric values. Thus, the temporal response of the spatial longitudinal mode in TMILC is temporally harmonic, or subharmonic, or bicritical accordingly as the temporal response of the modulated RBC is harmonic, or subharmonic, or bicritical.

Although the marginal instability curves for the transverse perturbations in TMILC are found to consist of a pattern of alternating harmonic and subharmonic regions in the space of the wave number of the perturbations and the Grashof number, the temporal response of TMILC in this case in the form of harmonic, or subharmonic, or bicritical responses further depends upon the angle of inclination of the layer with respect to the horizontal.

The onset mode of TMILC is found to occur in the form of a time periodically oscillating pattern of convective rolls, which corresponds to any of the following modes: LH, LS, TH, TS, TH-LH, TS-LH, TH-LS, TH-TS-LH, TH-LS-TH, depending upon the orientation of the layer with respect to the horizontal and modulation parameters. Modulation effects are significant for low to moderate forcing frequencies, and they are negligible for sufficiently large frequencies.

Except in a neighborhood of the angle of inclination for the codimension-2 point, modulation delays the onset of the longitudinal mode of TMILC and modulation favors the onset of the transverse mode of TMILC.

The angle of inclination for the codimension-2 point is also a function of the modulation parameters and Prandtl number of the fluid. The rate of variation of the angle of inclination for the codimension-2 point with the Prandtl number is significant for low Prandtl number fluids.

The present analysis of TMILC is mainly focused on investigating the effect of modulation on the value of the angle of inclination of the fluid layer with respect to the horizontal below which the preferred onset mode of TMILC is longitudinal and above which the preferred onset mode is transverse. For such an inclination, Floquet theory allows us to further classify the nature of the onset of the instability in the form of a time-periodic flow among the harmonic and the subharmonic types.

ACKNOWLEDGMENTS

The author is indebted to the learned referees for their helpful comments and constructive criticism in improving the overall quality of the article. The present research work is supported by Science and Engineering Research Board (SERB), Government of India under MATRICS Scheme wide project Grant No. MTR/2017/000575 awarded to the author.

APPENDIX

To define various matrices and block matrices, we proceed as follows: Let O and I , respectively, denote the zero matrix and the identity matrix each of order $N \times N$. Furthermore, for $X_n, Y_j \in \mathcal{L}^2(-\frac{1}{2}, \frac{1}{2})$ with $1 \leq n, j \leq N$, we define $\langle X_n, Y_j \rangle$ as the $N \times N$ matrix whose (n, j) th entry is equal to

$$\int_{-\frac{1}{2}}^{\frac{1}{2}} X_n(z) \overline{Y_j(z)} dz.$$

Having said this, the block matrix \mathbf{L}_ℓ for each $\ell = -L, -L + 1, \dots, L - 1, L$ appearing in Eq. (7) is given by

$$\mathbf{L}_\ell = \begin{pmatrix} L_1(\ell) - A_1 & O & O & O \\ O & L_2(\ell) - B_2 & O & O \\ O & -\langle \Psi_n, S_j \rangle & L_3(\ell) - C_3 & O \\ -\langle \Phi_n, C_j \rangle & O & O & L_4(\ell) - D_4 \end{pmatrix}, \quad (\text{A1})$$

where $h(z) = z(z^2 - \frac{1}{4})$ and

$$L_1(\ell) = \frac{i\omega(s + \ell)}{\sigma} (\langle \Phi_n'', \Phi_j \rangle - k^2 I), \quad (\text{A2})$$

$$L_2(\ell) = \frac{i\omega(s + \ell)}{\sigma} (\langle \Psi_n'', \Psi_j \rangle - k^2 I), \quad (\text{A3})$$

$$L_3(\ell) = L_4(\ell) = \frac{i\omega(s + \ell)}{2} I. \quad (\text{A4})$$

Further, the block matrices $\mathbf{U}_1, \mathbf{U}_2, \mathbf{V}$, and \mathbf{W} as in Eq. (7) are given by

$$\mathbf{U}_1 = k^2 \begin{pmatrix} O & O & O & \langle C_n, \Phi_j \rangle \\ O & O & \langle S_n, \Psi_j \rangle & O \\ O & O & O & O \\ O & O & O & O \end{pmatrix}, \quad (\text{A5})$$

$$\mathbf{U}_2 = \frac{k}{6} \begin{pmatrix} O & A_2 & 6A_3 & O \\ B_1 & O & O & 6B_4 \\ O & O & O & -\langle h(z)C_n, S_j \rangle \\ O & O & -\langle h(z)S_n, C_j \rangle & O \end{pmatrix}, \quad (\text{A6})$$

$$\mathbf{V} = \begin{pmatrix} O & O & O & O \\ O & O & O & O \\ O & G_2 & O & O \\ H_1 & O & O & O \end{pmatrix}, \quad (\text{A7})$$

$$\mathbf{W} = \frac{k}{2i\omega(1-\sigma)} \begin{pmatrix} O & E_2 & O & O \\ F_1 & O & O & O \\ O & O & O & \sigma G_4 \\ O & O & \sigma H_3 & O \end{pmatrix} \quad (\text{A8})$$

for $\sigma \neq 1$. Furthermore, the following matrices have been used in (A1)–(A6):

$$A_1 = \langle (\lambda_n^4 + k^4) \delta_{nj} \rangle - 2k^2 \langle \Phi_n'', \Phi_j \rangle, \quad (\text{A9})$$

$$A_2 = \frac{1}{\sigma} \{ \langle h(z) \Psi_n'', \Phi_j \rangle - \langle h''(z) \Psi_n, \Phi_j \rangle - k^2 \langle h(z) \Psi_n, \Phi_j \rangle \}, \quad (\text{A10})$$

$$A_3 = 2\pi \langle n \cos\{2n\pi z\}, \Phi_j \rangle, \quad (\text{A11})$$

$$B_1 = \frac{1}{\sigma} \{ \langle h''(z) \Phi_n, \Psi_j \rangle - \langle h(z) \Phi_n'', \Psi_j \rangle + k^2 \langle h(z) \Phi_n, \Psi_j \rangle \}, \quad (\text{A12})$$

$$B_2 = \langle (\mu_n^4 + k^4) \delta_{nj} \rangle - 2k^2 \langle \Psi_n'', \Psi_j \rangle, \quad (\text{A13})$$

$$B_4 = \pi \langle (2n-1) \sin\{(2n-1)\pi z\}, \Psi_j \rangle, \quad (\text{A14})$$

$$C_3 = -\frac{1}{2} \langle (4\pi^2 n^2 + k^2) \delta_{nj} \rangle, \quad (\text{A15})$$

$$D_4 = -\frac{1}{2} \langle ((2n-1)^2 \pi^2 + k^2) \delta_{nj} \rangle. \quad (\text{A16})$$

For $\sigma > 0$ and X_n, Y_j in $\mathcal{L}^2(-\frac{1}{2}, \frac{1}{2})$, we define $\langle M_\sigma(X_n, Y_j) \rangle$ and $\langle N_\sigma(X_n, Y_j) \rangle$ as the $N \times N$ matrices whose (n, j) th entries are $\int_{-1/2}^{1/2} f_\sigma(z, \omega) X_n(z) \overline{Y_j(z)} dz$ and $\int_{-1/2}^{1/2} X_n(z) (\frac{\partial}{\partial z} f_\sigma(z, \omega)) \overline{Y_j(z)} dz$, respectively. Consequently, each of the following $N \times N$ matrices is used in (A7) and (A8):

$$E_2 = \left(\frac{i\omega}{\sigma} + k^2 \right) \langle M_\sigma(\Psi_n, \Phi_j) \rangle - \langle M_\sigma(\Psi_n'', \Phi_j) \rangle + \langle M_1(\Psi_n'', \Phi_j) \rangle - (i\omega + k^2) \langle M_1(\Psi_n, \Phi_j) \rangle, \quad (\text{A17})$$

$$F_1 = -\left(\frac{i\omega}{\sigma} + k^2 \right) \langle M_\sigma(\Phi_n, \Psi_j) \rangle + \langle M_\sigma(\Phi_n'', \Psi_j) \rangle + (i\omega + k^2) \langle M_1(\Phi_n, \Psi_j) \rangle - \langle M_1(\Phi_n'', \Psi_j) \rangle, \quad (\text{A18})$$

$$G_2 = -\frac{1}{2} \langle N_1(\Psi_n, \mathcal{S}_j) \rangle, \quad (\text{A19})$$

$$G_4 = -\langle M_1(\mathcal{C}_n, \mathcal{S}_j) \rangle + \langle M_\sigma(\mathcal{C}_n, \mathcal{S}_j) \rangle, \quad (\text{A20})$$

$$H_1 = -\frac{1}{2} \langle N_1(\Phi_n, \mathcal{C}_j) \rangle, \quad (\text{A21})$$

$$H_3 = \langle M_1(\mathcal{S}_n, \mathcal{C}_j) \rangle - \langle M_\sigma(\mathcal{S}_n, \mathcal{C}_j) \rangle. \quad (\text{A22})$$

-
- [1] D. J. Tritton, Transition to turbulence in the free convection boundary layers on an inclined heated plate, *J. Fluid Mech.* **16**, 417 (1963).
- [2] W. T. Kierkus, An analysis of laminar free convection flow and heat transfer about an inclined isothermal plate, *Int. J. Heat Mass Transf.* **11**, 241 (1968).
- [3] E. M. Sparrow and R. B. Husar, Longitudinal vortices in natural convection flow on inclined plates, *J. Fluid Mech.* **37**, 251 (1969).
- [4] J. R. Lloyd and E. M. Sparrow, On the instability of natural convection flow on inclined plates, *J. Fluid Mech.* **42**, 465 (1970).
- [5] R. M. Clever, Finite amplitude longitudinal convection rolls in an inclined layer, *J. Heat Trans.* **95**, 407 (1973).
- [6] K. G. T. Hollands, T. E. Unny, G. D. Raithby, and L. Konicek, Free convective heat transfer across inclined air layers, *J. Heat Trans.* **98**, 189 (1976).
- [7] R. M. Clever and F. H. Busse, Instabilities of longitudinal convection rolls in an inclined layer, *J. Fluid Mech.* **81**, 107 (1977).
- [8] I. Hideo, Experimental study of natural convection in an inclined air layer, *Int. J. Heat Mass Transf.* **27**, 1127 (1984).
- [9] S. Chandrasekhar, *Hydrodynamic and Hydromagnetic Stability* (Oxford University Press, Oxford, 1966).
- [10] P. G. Drazin and W. H. Reid, *Hydrodynamic Stability* (Cambridge University Press, Cambridge, England, 2004).
- [11] E. L. Koschmieder, *Bénard Cells and Taylor Vortices* (Cambridge University Press, Cambridge, UK, 1993).
- [12] E. Bodenschatz, W. Pesch, and G. Ahlers, Recent developments in Rayleigh-Bénard convection, *Annu. Rev. Fluid Mech.* **32**, 709 (2000).
- [13] G. K. Batchelor, Heat transfer by free convection across a closed cavity between vertical boundaries at different temperatures, *Quart. Appl. Math.* **12**, 209 (1954).
- [14] C. M. Vest and V. S. Arpaci, Stability of natural convection in a vertical slot, *J. Fluid Mech.* **36**, 1 (1969).
- [15] A. Chait and S. A. Korpela, The secondary flow and its stability for natural convection in a tall vertical enclosure, *J. Fluid Mech.* **200**, 189 (1989).
- [16] S. A. Korpela, D. Gözum, and C. B. Baxi, On the stability of the conduction regime of natural convection in a vertical slot, *Int. J. Heat Mass Transf.* **16**, 1683 (1973).
- [17] R. F. Bergholz, Instability of steady natural convection in a vertical fluid layer, *J. Fluid Mech.* **84**, 743 (1978).
- [18] S. A. Suslov, Thermomagnetic convection in a vertical layer of ferromagnetic fluid, *Phys. Fluids* **20**, 084101 (2008).
- [19] J. E. Hart, Stability of the flow in a differentially heated inclined box, *J. Fluid Mech.* **47**, 547 (1971).
- [20] K. E. Daniels, B. B. Plapp, and E. Bodenschatz, Pattern Formation in Inclined Layer Convection, *Phys. Rev. Lett.* **84**, 5320 (2000).

- [21] P. Subramanian, O. Brausch, K. E. Daniels, E. Bodenschatz, T. M. Schneider, and W. Pesch, Spatio-temporal patterns in inclined layer convection, *J. Fluid Mech.* **794**, 719 (2016).
- [22] F. Reetz and T. M. Schneider, Invariant states in inclined layer convection. part 1. temporal transitions along dynamical connections between invariant states, *J. Fluid Mech.* **898**, A22 (2020).
- [23] F. Reetz, P. Subramanian, and T. M. Schneider, Invariant states in inclined layer convection. part 2. bifurcations and connections between branches of invariant states, *J. Fluid Mech.* **898**, A23 (2020).
- [24] L. S. Tuckerman, Ricocheting inclined layer convection states, *J. Fluid Mech.* **900**, F1 (2020).
- [25] M. Arora, J. Singh, and R. Bajaj, Nonlinear stability of natural convection in an inclined fluid layer, *Int. J. Appl. Comput. Math.* **6**, 21 (2020).
- [26] W. S. Edwards and S. Fauve, Patterns and quasi-patterns in the Faraday experiment, *J. Fluid Mech.* **278**, 123 (1994).
- [27] T. Besson, W. S. Edwards, and L. S. Tuckerman, Two-frequency parametric excitation of surface waves, *Phys. Rev. E* **54**, 507 (1996).
- [28] H. Arbell and J. Fineberg, Pattern formation in two-frequency forced parametric waves, *Phys. Rev. E* **65**, 036224 (2002).
- [29] W. Batson, F. Zoueshtiagh, and R. Narayanan, Two-frequency excitation of single-mode Faraday waves, *J. Fluid Mech.* **764**, 538 (2015).
- [30] J. Singh and R. Bajaj, Temperature modulation in Rayleigh-Bénard convection, *ANZIAM J.* **50**, 231 (2008).
- [31] B. L. Smorodin and M. Lücke, Convection in binary mixtures with modulated heating, *Phys. Rev. E* **79**, 026315 (2009).
- [32] J. Singh and R. Bajaj, Temperature modulation in ferrofluid convection, *Phys. Fluids* **21**, 064105 (2009).
- [33] J. Singh and R. Bajaj, Convective instability in a ferrofluid layer with temperature-modulated rigid boundaries, *Fluid Dyn. Res.* **43**, 025502 (2011).
- [34] J. Singh, R. Bajaj, and P. Kaur, Bicritical states in temperature-modulated Rayleigh-Bénard convection, *Phys. Rev. E* **92**, 013005 (2015).
- [35] P. Kaur, J. Singh, and R. Bajaj, Rayleigh-Bénard convection with two-frequency temperature modulation, *Phys. Rev. E* **93**, 043111 (2016).
- [36] P. Kaur and J. Singh, Heat transfer in thermally modulated two-dimensional Rayleigh Bénard convection, *Int. J. Therm. Sci.* **114**, 35 (2017).
- [37] A. Farooq and G. M. Homsy, Linear and nonlinear dynamics of a differentially heated slot under gravity modulation, *J. Fluid Mech.* **313**, 1 (1996).
- [38] U. E. Volmer and H. W. Müller, Quasiperiodic patterns in Rayleigh-Bénard convection under gravity modulation, *Phys. Rev. E* **56**, 5423 (1997).
- [39] R. Bajaj, Thermodiffusive magneto convection in ferrofluids with two-frequency gravity modulation, *J. Magn. Magn. Mater.* **288**, 483 (2005).
- [40] W. Y. Chen and C. F. Chen, Effect of gravity modulation on the stability of convection in a vertical slot, *J. Fluid Mech.* **395**, 327 (1999).
- [41] C. B. Baxi, V. S. Arpaci, and C. M. Vest, Stability of natural convection in an oscillating vertical slot, in *Proceedings of the Heat Transfer and Fluid Mechanics Institute*, edited by L. R. Davis and R. E. Wilson (Stanford University Press, Stanford, CA, 1974), pp. 171–183.
- [42] J. Singh and R. Bajaj, Stability of temperature modulated convection in a vertical fluid layer, *Appl. Math. Model.* **61**, 408 (2018).
- [43] J. Singh, P. Kaur, and R. Bajaj, Bicritical states in a vertical layer of fluid under two frequency temperature modulation, *Phys. Rev. E* **101**, 023109 (2020).
- [44] S. H. Davis, The stability of time periodic flows, *Annu. Rev. Fluid Mech.* **8**, 57 (1976).
- [45] J. Miles and D. Henderson, Parametrically forced surface waves, *Annu. Rev. Fluid Mech.* **22**, 143 (1990).
- [46] K. Kumar and L. S. Tuckerman, Parametric instability of the interface between two fluids, *J. Fluid Mech.* **279**, 49 (1994).
- [47] G. Z. Gershuni and E. M. Zhukhovitskii, Stability of plane-parallel convective motion with respect to spatial perturbations, *J. Appl. Math. Mech.* **33**, 830 (1969).
- [48] S. A. Korpela, A study on the effect of Prandtl number on the stability of the conduction regime of natural convection in an inclined slot, *Int. J. Heat Mass Transf.* **17**, 215 (1974).
- [49] Y. M. Chen and A. J. Pearlstein, Stability of free-convection flows of variable-viscosity fluids in vertical and inclined slots, *J. Fluid Mech.* **198**, 513 (1989).